# **Inorganic Chemistry**

pubs.acs.org/IC Article

## Synthesis of Type II Ge and Ge—Si Alloyed Clathrates Using Solid-State Electrochemical Oxidation of Zintl Phase Precursors

Andrew Dopilka, Alexander Ovchinnikov, Amanda Childs, Svilen Bobev, Xihong Peng, and Candace K. Chan\*



Cite This: Inorg. Chem. 2022, 61, 12363-12372



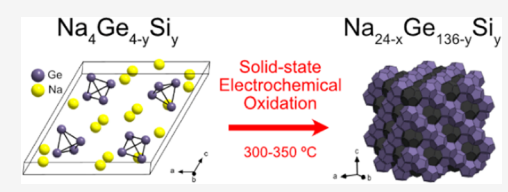
**ACCESS** I

Metrics & More

Article Recommendations

s Supporting Information

**ABSTRACT:** Germanium clathrates with the type II structure are open-framework materials that show promise for various applications, but the difficulty of achieving phase-pure products via traditional synthesis routes has hindered their development. Herein, we demonstrate the synthesis of type II Ge clathrates in a two-electrode electrochemical cell using  $Na_4Ge_{4-y}Si_y$  (y=0, 1) Zintl phase precursors as the working electrode, Na metal as the counter/reference electrode, and Na-ion conducting  $\beta''$ -alumina as the solid electrolyte. The galvanostatic



oxidation of  $Na_4Ge_4$  resulted in voltage plateaus around 0.34-0.40~V vs  $Na/Na^+$  with the formation of different products depending on the reaction temperature. When using  $Na_4Ge_3Si$  as a precursor, nearly phase-pure, alloyed type II Ge-Si clathrate was obtained at 350 °C. The Na atoms in the large  $(Ge,Si)_{28}$  cages of the clathrate occupied off-centered positions according to Rietveld refinement and density functional theory calculations. The results indicate that electrochemical oxidation of Zintl phase precursors is a promising pathway for synthesizing Ge clathrates with type II structure and that Si alloying of the Zintl phase precursor can promote selective clathrate product formation over other phases.

#### 1. INTRODUCTION

Tetrel (Tt = group 14 element) clathrates are a class of host guest materials with a myriad of interesting optical, electronic, and electrochemical properties due to their wide compositional and structural space. Different structure types of clathrates (type I, type II, type III, etc.) are discerned by the specific arrangement of the host atoms and the topology of the guest framework. The Tt framework structure can be described in terms of large polyhedra, often referred to as cages, that share common faces to form a three-dimensional (3D) network, with guest atoms occupying the centers of the polyhedra. For example, the type II structure is described by the Fd3m space group and has a general formula of  $M_{24}Tt_{136}$  (M = guest atoms) with face-sharing dodecahedra  $(Tt_{20})$  and hexakaidecahedra  $(Tt_{28})$  (Figure 1). Due to their ability to form frameworks without guest atoms, type II Si and Ge clathrates are of particular interest for thermoelectric, photovoltaic, hotovoltaic, hotovoltaic, and Li-ion battery<sup>7-9</sup> applications. For instance, the guest-free Si<sub>136</sub> and Ge<sub>136</sub> clathrates have direct or nearly direct band gaps of 1.9 and 0.6 eV, respectively, which can be tuned through alloying of the two structures.<sup>3</sup> Recently, we reported evidence of reversible Li insertion into guest-free type II Si<sub>136</sub> clathrates, and propose that similar behavior might be present in type II Ge<sub>136</sub> on the basis of its analogous structure. However, synthesis of the type II Ge clathrate phase has been more elusive; this is because the traditional synthetic approach for type II Si clathrates, thermal decomposition of the Na<sub>4</sub>Si<sub>4</sub> Zintl phase under vacuum, 10,11 is more difficult for the Ge analogue (Na<sub>4</sub>Ge<sub>4</sub>) and generally results in the formation of many phases (Figure 1).  $^{12}$  Recently, the selective growth of the type II Ge phase via thermal decomposition has been accomplished with specially designed reactors  $^{13}$  or via thin-film growth methods.  $^{14-16}$ 

To address this synthetic challenge, several novel approaches to prepare type II Ge clathrates have been investigated. On the basis that the oxidation state of Ge in the clathrate phase is close to zero, reactions involving oxidation of Ge anions are used to form clathrates. For instance, Guloy et al. first showed that guest-free type II Ge clathrate could be synthesized by chemical oxidation of [Ge<sub>9</sub>]<sup>4-</sup> clusters from Na<sub>4</sub>Ge<sub>9</sub> in an ionic liquid;1/ similar approaches were later reported via oxidation of  $K_4Ge_9^{18}$  and  $Na_{12}Ge_{17}^{19,20}$  with the latter precursor containing both [Ge<sub>9</sub>]<sup>4-</sup> and [Ge<sub>4</sub>]<sup>4-</sup> cluster anions.<sup>21</sup> A difficulty associated with the above chemical oxidation approaches is that the ionic liquids must have the appropriate functional groups to display redox behavior toward the anion clusters, or be able to generate stronger oxidizers such as HCl or alkyl chlorides in situ.20 The key feature of these methods is that the strength of the oxidizing agent must be tuned to optimize the conversion of the Zintl phase precursor(s) into the clathrate product.

Received: May 20, 2022 Published: July 25, 2022





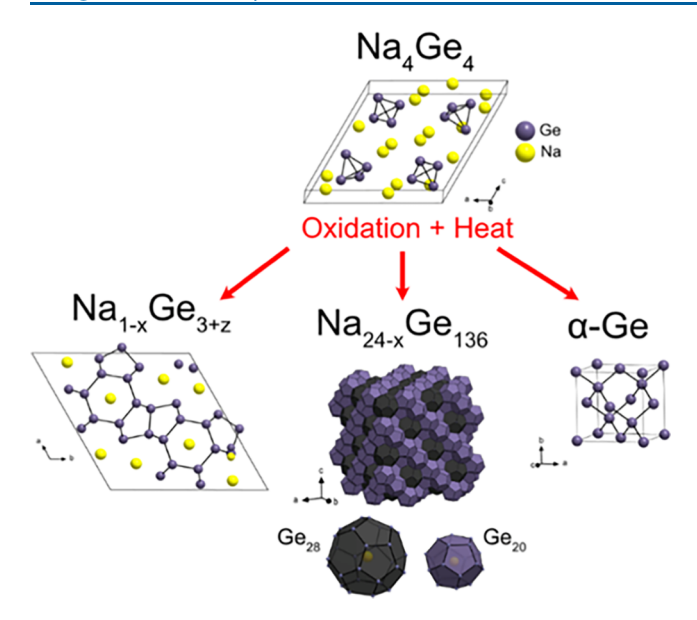


Figure 1. Crystal structure of  $Na_4Ge_4$  ( $P2_1/c$ ) along with the structures of reported products after oxidation that include hexagonal  $Na_{1-x}Ge_{3+z}$ , type II Ge clathrate ( $Fd\overline{3}m$ ) in polyhedral representation with the two types of polyhedra underneath: the hexakaidecahedra ( $Ge_{28}$ , black) and the dodecahedra ( $Ge_{20}$ , purple); and diamond cubic Ge ( $\alpha$ -Ge).

Compared to chemical methods, electrochemical methods have the advantage of offering more direct control of the oxidation reactions through tuning of the electrochemical potential. Recently, potentiostatic electrochemical oxidation (i.e., desodiation) of Na<sub>12</sub>Ge<sub>17</sub> in a LiI-NaI-CsI molten salt electrolyte at 280 °C was shown to preferably yield type II Ge clathrates (Na<sub>24-x</sub>Ge<sub>136</sub>).<sup>22</sup> However, the said process, following washing and careful analysis of the products, was demonstrated to allow the formation of both Na-filled (major phase) as well as Cs-filled Ge clathrate (minor phase), which could be due to cation exchange (Cs → Na) during the reaction.<sup>22</sup> It is therefore apparent that due to the conditions of the experiment and the high reactivity of the Zintl phase precursor, one needs to use an electrolyte that exhibits high ionic conductivity but is still stable at elevated temperatures. Meeting these requirements will be pivotal to the success of the electrochemical synthesis of the type II Ge clathrate.

Not long ago, our team reported on an electrochemical method to synthesize Na-filled Si clathrates using a Na-ion

conducting  $\beta''$ -Al<sub>2</sub>O<sub>3</sub> solid electrolyte in a cell geometry similar to that used in a Na-S battery.<sup>23</sup> The Zintl phase Na<sub>4</sub>Si<sub>4</sub> precursor was converted into Na<sub>8</sub>Si<sub>46</sub> clathrate with type I structure under constant current oxidation conditions via a solid-state, two-phase reaction. The electrochemical oxidation method allows for galvanostatic control over the reaction kinetics and in situ observation of the electrode potential during the reaction, which can allow for better understanding of the reaction mechanisms. Furthermore, the use of the Na+conducting solid electrolyte eliminates the possibility of cation exchange or the need for postsynthesis washing to remove ionic liquid or salt residues, unlike the other aforementioned (electro)chemical synthetic methods. To further evaluate the versatility of our method, herein, we investigate, for the first time, the solid-state electrochemical oxidation of Na<sub>4</sub>Ge<sub>4</sub> and alloyed Na<sub>4</sub>Ge<sub>3</sub>Si Zintl phases at various temperatures (300– 400 °C) toward the objective of synthesizing Ge and alloyed Ge-Si clathrates.

We find that the electrochemical oxidation products are temperature-dependent, with the type II Ge clathrate preferably forming from the Na<sub>4</sub>Ge<sub>4</sub> precursor at a lower temperature (300 °C), hexagonal Na<sub>1-x</sub>Ge<sub>3+z</sub> at an intermediate temperature (350 °C), and diamond cubic  $\alpha$ -Ge at a higher temperature (400 °C). When using Na<sub>4</sub>Ge<sub>3</sub>Si as a precursor, single-phase products were observed (type II clathrate at 350 °C and  $\alpha$ -Ge at 400 °C), suggesting that Si alloying with the precursor can improve the phase purity. X-ray diffraction analysis suggests that Na atoms are found in offcenter positions in the larger cages of the alloyed type II Ge-Si clathrate, which is supported by density functional theory (DFT) calculations. Overall, this work further demonstrates the viability of using electrochemical methods to synthesize clathrates via the controlled oxidation of the Zintl phase precursors.

## 2. EXPERIMENTAL AND COMPUTATIONAL METHODS

The electrochemical synthesis was carried out in a home-built cell encased in a stainless-steel housing (Figure 2a) using a design adapted from our previous setup that was used to synthesize Si clathrates from Na<sub>4</sub>Si<sub>4</sub> precursors.<sup>23</sup> The cell design was modified to simplify the cell assembly procedure and provide a more reliable way to apply pressure to the electrodes. Figure S1a shows a photograph of the cell and more detailed descriptions of the cell assembly can be found in the Supporting Information. Two differently sized boron nitride (BN) crucibles were used as the basis of the cell (Figure S1b). A spring in

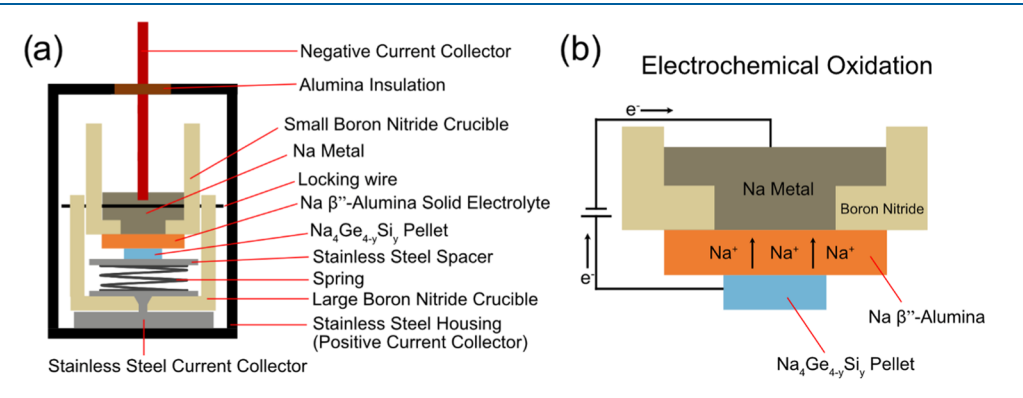


Figure 2. (a) Schematic of the two-electrode cell used to perform the electrochemical oxidation of the  $Na_4Ge_{4-y}Si_y$  (y=0,1) Zintl phase precursors; (b) schematic of the electrochemical oxidation process showing the movement of Na ions and electrons during oxidation of the  $Na_4Ge_{4-y}Si_y$  pellet.

the bottom of the larger BN crucible allows for pressure to be applied to the working electrode (WE, a pellet of Na<sub>4</sub>Ge<sub>4</sub> or Na<sub>4</sub>Ge<sub>3</sub>Si), which was positioned in between a stainless-steel disk and Na  $\beta''$ -alumina solid electrolyte disc. Then, Na metal, which acts as the reference/counter electrode (RE/CE), was contacted to the solid electrolyte to form the two-electrode cell. The movement of electrons and Na<sup>+</sup> ions during the oxidation process is shown schematically in Figure 2b. Prior to application of any current, the cell was heated at 450 °C for 20 h and then the temperature was reduced to the desired reaction temperature afterward. The  $\beta''$ -Al<sub>2</sub>O<sub>3</sub> solid electrolyte has notable issues with Na metal wetting at lower temperatures (300 °C) and thus the hold at 450 °C is used to ensure good wetting of the Na metal with the solid electrolyte. <sup>24</sup> Figure S1c shows the Na metal electrode contacting the solid electrolyte with good wetting after a reaction involving the 450 °C hold.

To carry out the electrochemical oxidation, we used the galvanostatic intermittent titration technique (GITT), which involves current pulses with time for open-circuit relaxation. The purpose of using the GITT method is to observe the open-circuit potential after each relaxation period to remove kinetic effects on the potential of the system. The cell polarization is seen from the difference between the steady-state open-circuit potential after relaxation and the potential during the galvanostatic pulse. After each reaction was completed, the cell was cooled and then disassembled, and the products were retrieved and characterized with powder X-ray diffraction (PXRD) and scanning electron microscopy (SEM) with energy-dispersive X-ray spectroscopy (EDS).

First-principles DFT calculations were performed in a similar manner to our previous work. <sup>26–28</sup> The Gibbs free energy change and average sodiation voltages were calculated as described previously. <sup>26,28</sup> The climbing image nudged elastic band (NEB) method was used to calculate Na migration barriers. <sup>29</sup> More details about the synthesis, electrochemical characterization, materials characterization, and computational methods are in the Supporting Information.

#### 3. RESULTS AND DISCUSSION

Figure 3 shows the GITT voltage profiles for the oxidation of  $Na_4Ge_4$  obtained at 300, 350, and 400 °C using 12 h long current pulses separated by 1 h rest periods, with the current densities indicated in each region. The current density of each pulse was halved from the previous one once the voltage started to increase sharply or reach 5 V vs  $Na/Na^+$ . The extent of reaction (*x*-axis of the voltage profiles) is shown as the desodiation capacity with respect to the original mass of  $Na_4Ge_4$  in the WE pellet. The vertical dotted lines at 231 and 280 mAh/g mark the theoretical capacities (see the Supporting Information for calculations) expected for desodiation of  $Na_4Ge_4$  to the final compositions of  $Na_24Ge_{136}$  and  $Ge_{136}$  respectively.

The cell voltage for the electrochemical oxidation of Na<sub>4</sub>Ge<sub>4</sub> at 300 °C started at close to 0.00 V vs Na/Na<sup>+</sup> and then increased gradually until plateauing at 0.50 V as the desodiation capacity increased (Figure 3a). Because this is a two-component system at constant pressure and temperature, the initial varying potential is indicative of a single-phase process.<sup>30</sup> This suggests that the Zintl phase precursor may have contained a slight excess of Na, which was removed in this sloped region of the voltage profile. The subsequent voltage plateau indicates the presence of a two-phase process, suggesting the conversion of Na<sub>4</sub>Ge<sub>4</sub> to form a new phase. The equilibrium potential reached during the relaxation period after the first current pulse was 0.40 V and can be assigned to the voltage for conversion of Na<sub>4</sub>Ge<sub>4</sub> to the products; this is notably higher than the potential for the conversion of Na<sub>4</sub>Si<sub>4</sub> to Si clathrate products (57 mV at 550 °C) observed in our previous study.<sup>23</sup> The higher voltage seen in the Ge system is

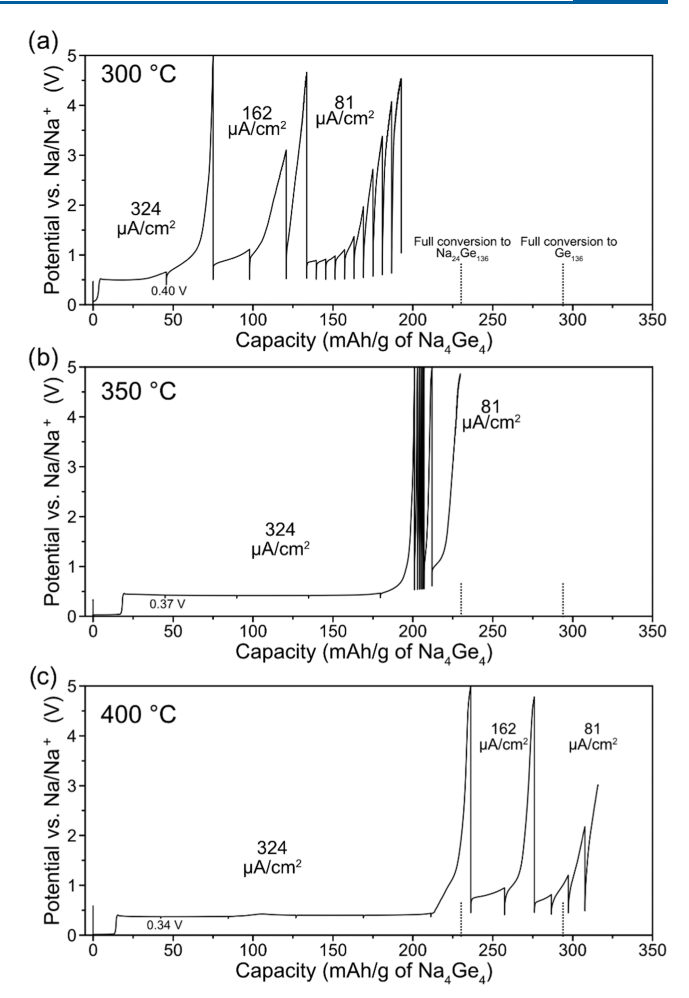


**Figure 3.** Galvanostatic intermittent titration technique (GITT) voltage profile of the electrochemical oxidation of  $Na_4Ge_4$  at (a) 300, (b) 350, and (c) 400 °C with 12 h long current pulses and 1 h of relaxation time between pulses. The dotted lines at the bottom represent the theoretical capacities for converting  $Na_4Ge_4$  to  $Na_{24}Ge_{136}$  and to  $Ge_{136}$ , respectively (see the Supporting Information for capacity calculations).

consistent with DFT calculations of the voltages of Na<sub>4</sub>Ge<sub>4</sub> and Na<sub>4</sub>Si<sub>4</sub> (~0.38 V compared to ~50 mV vs Na/Na<sup>+</sup>, respectively).<sup>31</sup> After the first current pulse, the cell potential quickly increased and so the current density was lowered sequentially until a capacity of 190 mAh/g was attained, which is lower than the capacity (231 mAh/g) needed for full conversion of the precursor to Na<sub>24</sub>Ge<sub>136</sub>. The steady-state voltage observed in the relaxation periods between the current pulses remained similar during the entire desodiation process despite the large rise in cell polarization, suggesting the occurrence of a two-phase reaction; this is similar to that observed in the oxidation of  $Na_4Si_4$ . Figure 3b shows the GITT voltage profile for the reaction at 350 °C, which shows much lower polarizations and a flatter plateau with a steadystate voltage of 0.37 V in the relaxation. In this case, the beginning of the profile shows a flat plateau near 0.00 V, which could be from the presence of Na metal in the WE pellet, since excess Na was used in the synthesis of Na<sub>4</sub>Ge<sub>4</sub> to ensure full reaction of the Ge and the potential of an electrochemical cell is zero when there is no difference in chemical potential at the two electrode/electrolyte interfaces. The cell polarization was much lower at 350 °C than at 300 °C, suggesting that the

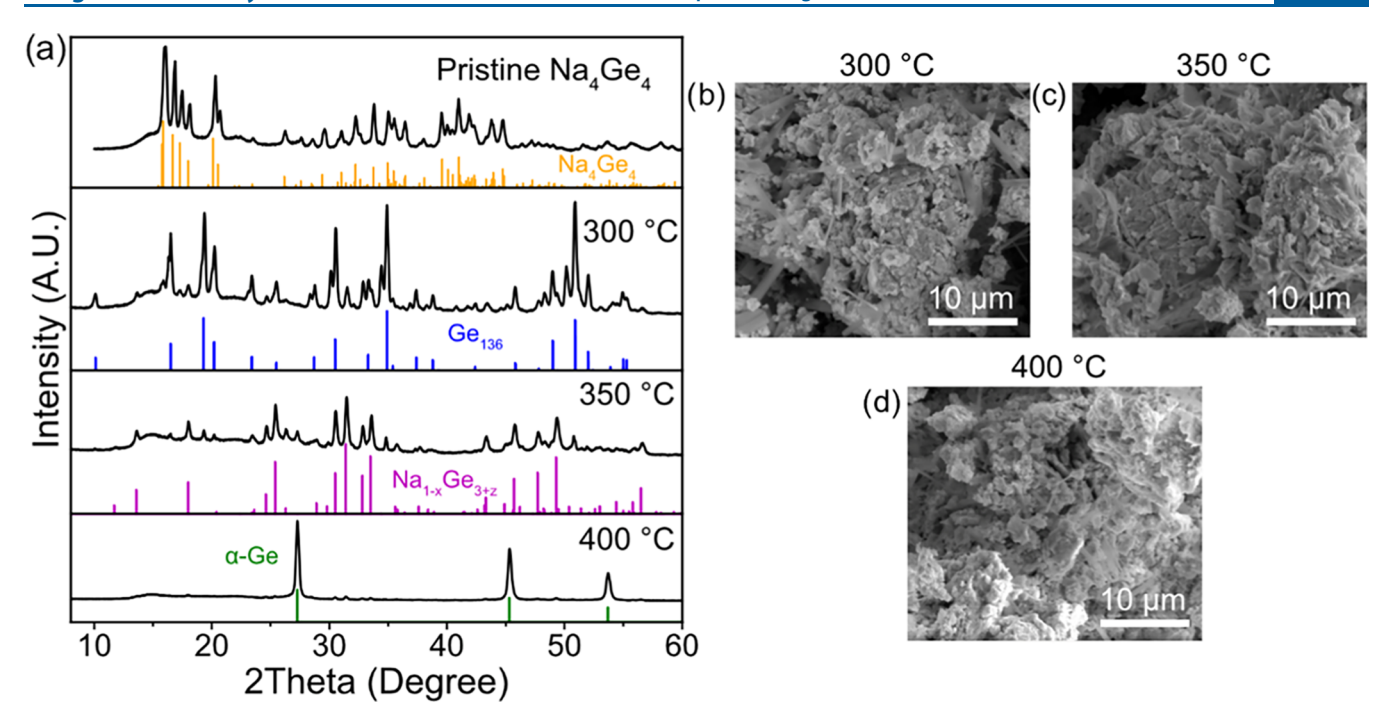


Figure 4. (a) PXRD of the pristine (as-prepared) Na<sub>4</sub>Ge<sub>4</sub> precursor and the reaction products synthesized at the indicated temperatures, along with the reference pattern for the majority product phase. The broad background from  $15 < 2\theta < 25^{\circ}$  is from the Kapton film used to protect the sample from reaction with air during the PXRD measurement. Na<sub>4</sub>Ge<sub>4</sub> reference structure from ref 41, Ge<sub>136</sub> from ref 17, and Na<sub>1-x</sub>Ge<sub>3+z</sub> from ref 35. SEM micrographs of the products after exposure to air at (b) 300, (c) 350, and (d) 400 °C.

temperature has a large effect on the kinetics of the reaction. The capacity for the reaction at 350 °C reached 240 mAh/g, which is close to that for full conversion to Na<sub>24</sub>Ge<sub>136</sub> (231 mAh/g). The voltage profile for the reaction at 400 °C is similar to that at 350 °C, but with a steady-state voltage after relaxation of 0.34 V. The cell reaches a higher capacity (320 mAh/g) than the one at 350 °C, indicating that desodiation of the Na<sub>24</sub>Ge<sub>136</sub> may have taken place; however, the total capacity is larger than what would be expected from the full removal of all of the Na to form empty Ge<sub>136</sub> (280 mAh/g). This suggests that there could be some self-discharge as described in our previous work, 23 which results from vaporization of the Na CE and its deposition onto the WE to reform Na<sub>4</sub>Ge<sub>4</sub>. Although the two electrodes are sealed away from each other and separated by the two BN crucibles and a solid electrolyte/BN interface, it could still be possible that some Na vapor is transporting between the interfaces to reach the WE. Indeed, formation of Na<sub>4</sub>Ge<sub>4</sub> via Na vapor reaction with Ge has been demonstrated to occur at 400 °C, 14 suggesting that this could be the cause of the excess observed capacity

The PXRD patterns of the pristine (as-prepared)  $Na_4Ge_4$  and the product of each reaction at different temperatures without exposure to air (using Kapton film to cover the powders) are presented in Figure 4a. The PXRD results show that in all of the reactions, the  $Na_4Ge_4$  had been consumed and new reflections from different crystalline phases were present. Interestingly, despite the similar voltage profiles observed in the electrochemical measurements, the product formed at each of the temperatures is very different. For the reaction performed at 300 °C, the product is predominately composed of type II Ge clathrates. There appears to be a small amount of  $Na_4Ge_4$  present based on the reflection at  $2\theta \sim 16^\circ$ , which is consistent with the lower capacity compared to the theoretical

capacity associated with complete conversion to Na24Ge136. The other identified reflections include two Na<sub>x</sub>Ge<sub>136</sub> clathrate phases with different lattice parameters (reflecting different Na contents) and a small amount of hexagonal Na<sub>1-x</sub>Ge<sub>3+z</sub>. Rietveld refinement (Figure S2 and Tables S1-S3) supports this assignment with a fit to three phases: 50.0 wt %  $Na_{0.3(1)}Ge_{136}$ , 27.9 wt %  $Na_{20.9(2)}Ge_{136}$ , and 22.1 wt % Na<sub>1</sub>Ge<sub>3.244</sub> (P6/m). The lattice parameters of Na<sub>20.9(2)</sub>Ge<sub>136</sub> match well with those for Na-filled type II Ge clathrate. For instance, the lattice constant for Na<sub>20.9(2)</sub>Ge<sub>136</sub> reported here is 15.4324(2) Å, while it was reported as 15.4355(4) Å for  $Na_{21.4(7)}Ge_{136}^{\phantom{1}20,32}$  and 15.4412(7) Å for  $Na_{23.0(5)}Ge_{136}^{\phantom{1}22}$ . The lattice constant for the nearly guest-free clathrate Na<sub>0.3(1)</sub>Ge<sub>136</sub> was 15.2363(1) Å, which is slightly larger than the lattice constant of Ge<sub>136</sub>, 15.2115(1) Å, reported previously.<sup>17</sup> Notably, unlike in other synthesis methods, 13,17,22 there appears to be no formation of  $\alpha$ -Ge as an impurity phase at 300 °C.

For the reaction performed at 350 °C, the major phase in the product was hexagonal  $Na_{1-x}Ge_{3+z}$  (Figure 1) with  $Na_xGe_{136}$  and  $\alpha$ -Ge as minor phases, while the major phase at 400  $^{\circ}\text{C}$  was  $\alpha\text{-Ge}$  with a minor contribution from the hexagonal  $Na_{1-x}Ge_{3+z}$  phase. These results show that the reaction temperature has a significant effect on the products that formed. At low temperatures, the type II clathrate phase is favored, which is consistent with the reaction temperatures of other synthesis methods. 13,14,17,22 The formation of hexagonal Na<sub>1-x</sub>Ge<sub>3+z</sub> at 350 °C with our electrochemical approach is also consistent with the synthesis temperature of this phase using thermal decomposition of Na<sub>4</sub>Ge<sub>4</sub> under dynamic vacuum (350–360 °C). 33 While the temperature dependence of the cell potential has not yet been elucidated because the temperature coefficient<sup>34</sup> for this reaction is unknown, the similarities of the voltage profiles in Figure 3 suggest that the

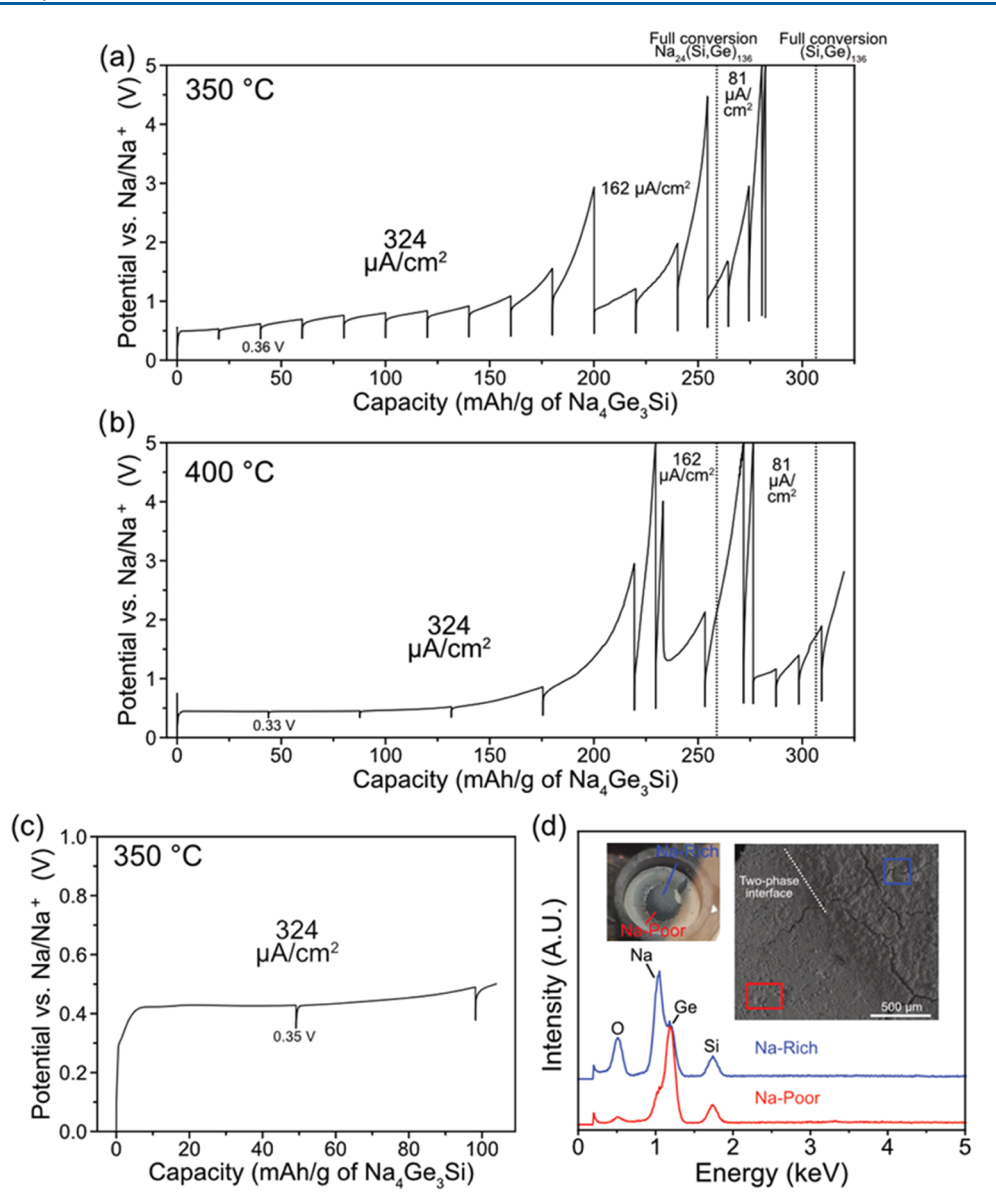


Figure 5. Galvanostatic intermittent titration technique (GITT) voltage profile of the electrochemical oxidation of  $Na_4Ge_3Si$  at (a) 350 and (b) 400 °C with 12 h long current pulses and 1 h of relaxation time. The dotted lines at the bottom represent the theoretical capacities for converting  $Na_4Ge_3Si$  to  $Na_{24}(Ge,Si)_{136}$  and to  $(Ge,Si)_{136}$ , respectively (see the Supporting Information for capacity calculations). (c) GITT voltage profile of the partial oxidation of  $Na_4Ge_3Si$  (33% of theoretical full oxidation) at 350 °C. (d) SEM EDS spectra of the area in the boxes marked in red and blue in the inset SEM image (top right) and a photograph of the pellet (top left inset) after partial oxidation showing the distinct two-phase boundary.

phases form at similar potentials and that the temperature is the main determiner of the phase formation.

SEM images of the reaction products obtained at each temperature (Figure 4b–d) show that the powders mainly consist of agglomerates of smaller particles in addition to particles with wirelike morphology. Interestingly, this wire morphology was seen in all of the samples, but its origin and composition is unknown. The EDS analysis of the powders did not reveal any obvious elemental impurities (Figure S3), suggesting that the wires could be one of the reaction products. Overall, the results demonstrate that the solid-state oxidation of  $Na_4Ge_4$  in an electrochemical cell can result in product formation analogous to those from other chemical oxidation methods, generally resulting in a multiphase product. The voltage profiles demonstrate the reactions proceed via two-phase reactions with potentials around 0.34-0.4~V vs  $Na/Na^+$ .

Next, a Na<sub>4</sub>Ge<sub>2</sub>Si pellet WE was oxidized in a similar way to investigate whether better product selection could be achieved since Baranowski et al. demonstrated that the phase purity of the type II phase product could be improved by alloying small amounts of either Ge or Si into their respective end member. 13 Figure 5a,b shows the voltage profiles for oxidation of Na<sub>4</sub>Ge<sub>3</sub>Si at 350 and 400 °C, with the dotted vertical lines showing the theoretical capacities for full conversion to the filled and empty type II alloyed clathrate, i.e., Na<sub>24</sub>(Ge,Si)<sub>136</sub> and (Ge,Si)<sub>136</sub>, respectively. The voltage profiles are similar to those obtained when using the Na<sub>4</sub>Ge<sub>4</sub> WE, with initial potential starting near 0.00 V vs Na/Na+ and quickly increasing and then plateauing. There was no initial plateau at 0.00 V in these experiments, suggesting that there was possibly less excess Na metal in the Na<sub>4</sub>Ge<sub>3</sub>Si precursor compared to in Na<sub>4</sub>Ge<sub>4</sub>. The steady-state voltages during the

relaxation periods were 0.36 and 0.33 V at 350 and 400  $^{\circ}$ C, respectively. These voltages are similar to those observed for the Na<sub>4</sub>Ge<sub>4</sub> precursor at the same temperatures, suggesting that the addition of Si to the Zintl precursor did not significantly change the reaction voltage. The final capacity at 350  $^{\circ}$ C was 285 mAh/g, which is greater than the capacity expected for forming the type II clathrate with composition of Na<sub>24</sub>Si<sub>34</sub>Ge<sub>102</sub> (261 mAh/g). Similarly, the final capacity for the reaction at 400  $^{\circ}$ C was 340 mAh/g, which is higher than the capacity corresponding to full removal of all of the Na atoms from the clathrate (317 mAh/g), suggesting that Na vapor might be self-discharging the cell. Overall, the voltage profiles for the oxidation of Na<sub>4</sub>Ge<sub>3</sub>Si show similar features to those for the oxidation of Na<sub>4</sub>Ge<sub>4</sub>.

To gain insight into the reaction process during electrochemical desodiation, partial oxidation of the Na<sub>4</sub>Ge<sub>3</sub>Si pellet was performed at 350 °C and the subsequent morphology and composition were investigated. Figure 5c shows the GITT voltage profile for the oxidation of Na<sub>4</sub>Ge<sub>3</sub>Si to 33% of the theoretical capacity needed to remove all of the available Na. Due to the two-phase reaction mechanism, the sample is expected to contain unreacted Na<sub>4</sub>Ge<sub>3</sub>Si coexisting with particles of products from the desodiation process. After cell disassembly, a two-phase boundary was observed from visual inspection of the pellet on the basis of the slight color difference (Figure 5d). The pellet was then investigated with SEM and EDS after brief exposure to air. The results show there is a distinct morphological and compositional difference between the two regions. The "Na-rich" region had a higher Na and O content compared to the "Na-poor" region. This Na-rich region is assigned to the unreacted Na<sub>4</sub>Ge<sub>3</sub>Si precursor, which is expected to contain more Na and display high reactivity to air, and hence the high oxygen content in the EDS spectrum. The Na-poor region is then assigned to the products of the electrochemical oxidation of Na<sub>4</sub>Ge<sub>3</sub>Si. Consistent with the flat voltage plateau in the GITT profile, the electrochemical reaction appears to proceed through a twophase boundary. Interestingly, the reaction front proceeds radially from the edge of the Na<sub>4</sub>Ge<sub>3</sub>Si pellet as opposed to perpendiculary from the face of the pellet that is in contact with the planar solid electrolyte interface. The origin of this behavior is currently unknown but could be due to a number of factors including stress evolution from volume change in the pellet, inhomogenous contact with the solid electrolyte, and/or location of the initial nucleation of the product phase in the WE pellet.

The PXRD patterns of the pristine Na<sub>4</sub>Ge<sub>3</sub>Si precursor and reaction products obtained after full reaction at 350 and 400 °C (no exposure to air) are shown in Figure 6 along with corresponding SEM micrographs. The PXRD results show that full conversion of the Zintl phase precursor was achieved along with the phase-pure synthesis of the type II clathrate phase at 350 °C and the  $\alpha$ -(Ge,Si) phase at 400 °C. Notably, there is no sign of the hexagonal Na<sub>1-x</sub>Ge<sub>3+z</sub> phase in the PXRD patterns, suggesting that the incorporation of Si into the Zintl phase precursor prevented the formation of this competing phase. SEM micrographs of the products show that the powders are composed of agglomerates of nanosized particles. The diamond cubic particles formed in the reaction at 400 °C are smaller than the clathrate particles formed at 350 °C, is consistent with the broadened PXRD peaks, which could be due to nanometer crystallite sizes, although a spread in lattice constants from the alloying could also be possible. The

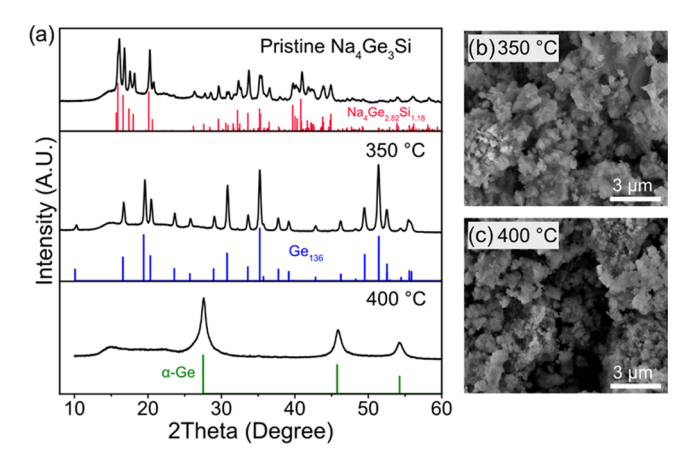


**Figure 6.** (a) PXRD pattern of pristine (as-prepared) Na<sub>4</sub>Ge<sub>3</sub>Si and the products of the reactions at 350 and 400 °C. SEM micrographs of the products after exposure to air at (b) 350 and (c) 400 °C. The broad background from  $15 < 2\theta < 25$ ° is from the Kapton film used to protect the sample from oxidation during the PXRD measurement. Na<sub>4</sub>Ge<sub>2.82</sub>Si<sub>1.18</sub> reference structure from ref 41, Ge<sub>136</sub> from ref 17.

morphology of these products is similar to what we observed previously in the electrochemical oxidation of  $Na_4Si_4$  to form Si clathrates. Another notable difference between the microstructure of the products resulting from oxidation of  $Na_4Ge_4$  and  $Na_4Ge_3Si$  is the absence of particles with wirelike morphology in the latter case, suggesting that the incorporation of Si significantly modified the resulting products. We speculate the wirelike particles may be composed of the hexagonal  $Na_{1-x}Ge_{3+z}$  phase, but no morphology information was reported in the previous studies 33,35,36 conducted on this material, and we did not investigate this further, as mentioned earlier.

To better elucidate the structure of the clathrate phase synthesized at 350 °C from the Na<sub>4</sub>Ge<sub>3</sub>Si precursor, Rietveld refinement was performed (Figure 7). First, the pattern was fit to a guest-free type II clathrate structure with the composition

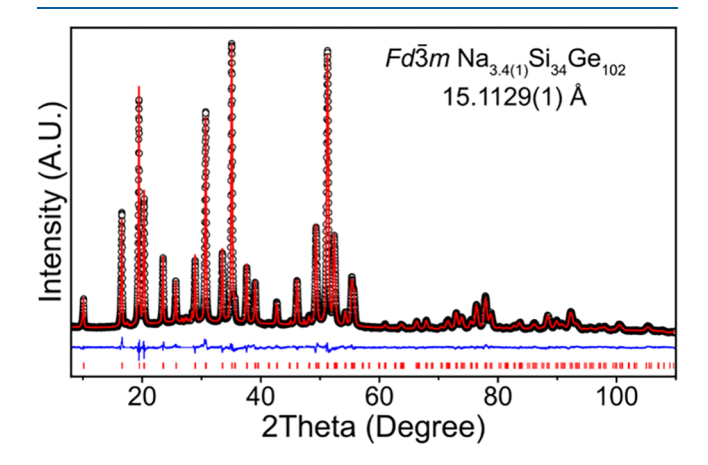


**Figure 7.** Rietveld refinement of the PXRD pattern for the type II clathrate product formed after oxidation of  $Na_4Ge_3Si$  at 350 °C after being exposed to air. Black circles represent the experimental pattern, the red curve represents the calculated pattern, and the blue curve represents the difference curve. The refined atomic positions, occupancies, and atomic displacement parameters can be found in Tables S4 and S5. The red tick marks represent the reflections corresponding to  $Na_{3,4(1)}Si_{34}Ge_{102}$ . Refinement residuals:  $\chi^2 = 2.07$ ,  $R_p = 0.028$ , and  $wR_p = 0.037$ .

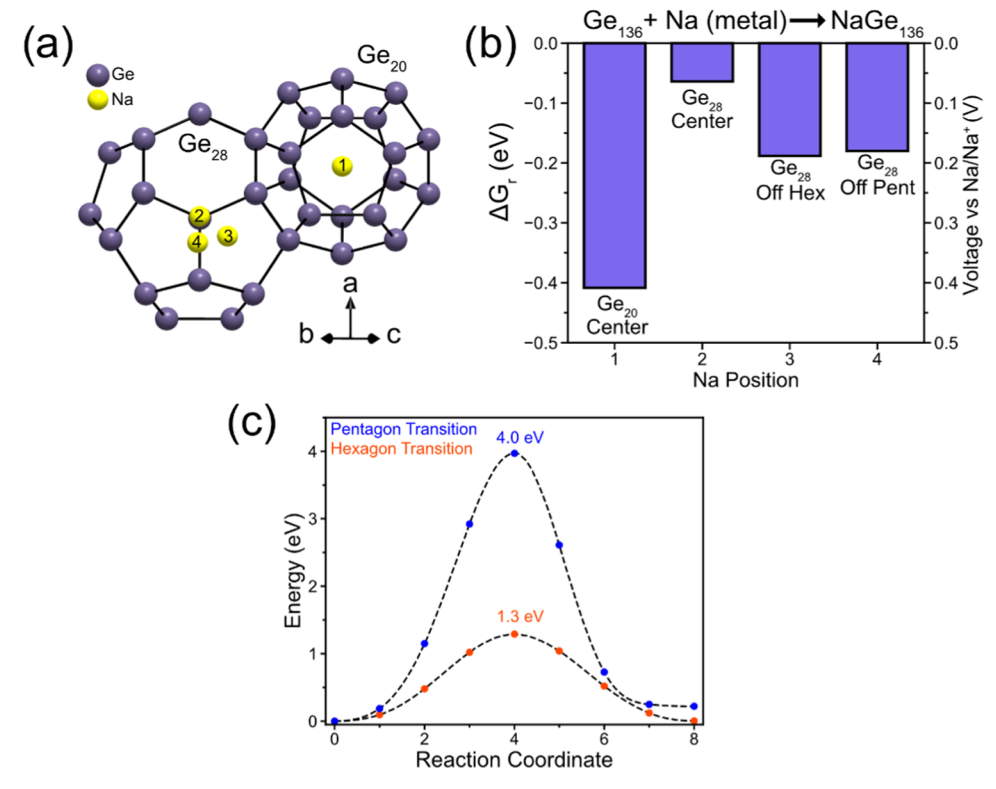


Figure 8. DFT calculation results of Na positions in  $Ge_{136}$  (a) Schematic of a  $Ge_{28}$  cage connected with a  $Ge_{20}$  cage showing the DFT-calculated Na positions viewed down the [110] direction. (b) Gibbs free energy of reaction ( $\Delta G_r$ ) for the reaction  $Ge_{136}$  + Na (metal)  $\rightarrow$  Na $Ge_{136}$  for each different Na position. (c) NEB-calculated minimum energy paths for migration of Na in  $Ge_{136}$  between the  $Ge_{20}$  and  $Ge_{28}$  cages through a shared pentagonal face (pentagon transition) and between the  $Ge_{28}$  and  $Ge_{28}$  cages through a shared hexagonal face (hexagon transition).

of Si<sub>34</sub>Ge<sub>104</sub>, assuming homogeneous mixing of the Si on the Ge framework sites. The ratio of Si and Ge was fixed to the nominal composition of the precursor, which was supported by the composition obtained from the EDS analysis of the powders (Figure S4). The lattice parameter was refined against a NIST Si standard (Figure S5) and determined to be 15.1129(1) Å, which is smaller than the lattice parameter of the guest-free Ge<sub>136</sub> (15.2115(1) Å) reported previously but similar to the lattice parameter for the alloyed Si<sub>0.25</sub>Ge<sub>0.75</sub> clathrate (15.10 Å), 13 thus confirming the incorporation of Si into the Ge lattice. After the pattern was fit to the guest-free structure, a difference Fourier transform was performed, which revealed residual electron density in both (Ge,Si)20 and (Ge,Si)<sub>28</sub> cages. In the smaller cages, a peak was found in the center, which is attributed to Na, while residual electron density in the larger cages was split to form a tetrahedron aligned around the four hexagonal faces of the hexakaidecahedra. The structure was refined with Na in the center of the (Ge,Si)<sub>20</sub> and in the off-center 32e Wyckoff position in the (Ge,Si)<sub>28</sub> cages with their displacement parameters fixed equal to the framework site. The refinement resulted in a final composition of Na<sub>3.4(1)</sub>Si<sub>34</sub>Ge<sub>102</sub>, suggesting that most of the Na had been removed by the electrochemical oxidation. The crystallographic information, atomic coordinates, and atomic displacement parameters are presented in Tables S4 and S5.

The off-centered Na positions aligned with the hexagonal faces in the large hexakaidecahedra are similar to those seen in our previous refinements<sup>9</sup> for Li within the Si<sub>28</sub> cages of type II Si clathrates and result from a mismatch between the cage size and the size of the cation. Since Na already has been demonstrated to occupy a slightly off-centered position in the

 $\mathrm{Si}_{28}$  cage,  $^{37,38}$  this effect is expected to be exacerbated in the larger  $(\mathrm{Ge},\mathrm{Si})_{28}$  cages. Although this disorder has been modeled with off-centered Na positions in the  $\mathrm{Si}_{28}$  cages, modeling Na with off-centered positions has yet to be considered for the  $\mathrm{Na}_{24-x}\mathrm{Ge}_{136}$  clathrate. Herein, we present structural evidence for the off-centered positions for Na atoms in the larger  $(\mathrm{Ge},\mathrm{Si})_{28}$  cages.

To further investigate the possible Na positions inside the Ge<sub>136</sub> host, DFT calculations were used following a similar methodology as reported in our previous work (Supporting Information). 9,28 Figure 8a shows a crystal model schematic of the investigated Na positions: the center of the Ge<sub>20</sub> (dodecahedra) and Ge28 (hexakaidecahedra) cages (indicated as positions 1 and 2, respectively), inside the Ge<sub>28</sub> cage and coordinated off of a hexagonal face (Off Hex, position 3) or pentagonal face (Off Pent, position 4). After relaxation, the Na atoms in positions 3 and 4 were found to be off-center by 1.311 and 1.195 Å, respectively. For comparison, the Na atoms in Si<sub>28</sub> were found, experimentally, to be 0.54 Å off-center.<sup>37</sup> Figure 8b shows the Gibbs free energy of reaction for each Na position relative to Na metal and the guest-free Ge<sub>136</sub>, where a more negative Gibbs free energy corresponds to a more favorable reaction and more positive average sodiation voltage.

The results show that the most favorable Na positions in the type II Ge clathrate lattice are in the center of the  $Ge_{20}$  cage and in the off-centered positions within the  $Ge_{28}$  cage. The center  $Ge_{28}$  cage position is 0.12 eV higher in energy than the Off Hex positions, suggesting that Na would prefer to occupy an off-center position in the large  $Ge_{28}$  cages. This is consistent with the results from the Rietveld refinement of the clathrate product from the oxidation of  $Na_4Ge_3Si$  obtained at 350 °C

(Figure 7). Despite the presence of 25% Si in the synthesized product, we expect a similar trend to that seen in the DFT results calculated for pure  $Ge_{136}$  since the energies associated with the guest atom positions are primarily dependent on the sizes of the cages.<sup>28</sup> The  $Ge_{28}$  cage is too large to maintain the favorable  $\sim$ 3.0 Å Na–Ge distance if Na occupies the cage center, and thus the Na atom prefers to be off-centered.

Since type II clathrates such as  $Na_{24-x}Ge_{136}$  can display variable Na content (0 < x < 24),  $^{20,22}$  the Na content is expected to be controlled by the bulk diffusion of Na through the clathrate lattice in a similar vein to Si<sub>136</sub>. Because empty clathrates are of more technological interest than the Na-filled ones, 9,13,17 understanding the kinetics and pathways of Na migration will be important for obtaining these guest-free structures. Figure 8c shows the energy vs reaction coordinate plots for nudged elastic band (NEB) calculations that were performed to determine the Na migration barriers between the two types of cages. The results show that when Na migrates between two Ge28 cages through a hexagonal face, the migration barrier is 1.3 eV, similar to the values we calculated previously for Na migration in the type I clathrate Ge<sub>46</sub> (1.5 eV).<sup>28</sup> For Na migration between the Ge<sub>28</sub> and Ge<sub>20</sub> cages through a pentagonal face, the migration barrier is much higher at 4.0 eV. Interestingly, the pathway did not converge to a path that resulted in breaking a Ge-Ge bond to lower the migration barrier of the pentagonal transition state. This phenomenon has been observed in a variety of situations for Li and Na migration in clathrates<sup>9,28,40</sup> and seems to be a possible mechanism for alkali metals to move in and out of the small dodecahedra with a lower migration barrier. It is possible that the transition state is only feasible if a Na atom is present in an adjacent cage so that migration through a cooperative mechanism can take place, similar to what we hypothesized can occur for Li migration in Si<sub>136</sub> and Si<sub>46</sub>. More calculations and experiments will be needed to elucidate this mechanism and the diffusion of Na within the Ge framework. The DFT calculations shown here support the experimental findings that the Na atoms prefer to adopt off-centered positions in the hexakaidecahedra and demonstrate that Na migration barriers are expected to be relatively high in type II Ge clathrates, consistent with the high temperatures needed to desodiate the structure.

#### 4. CONCLUSIONS

In this work, the solid-state electrochemical oxidation of Na<sub>4</sub>Ge<sub>4</sub> and Na<sub>4</sub>Ge<sub>3</sub>Si Zintl phase precursors were performed in a two-electrode cell containing a Na  $\beta''$ -alumina solid electrolyte. The GITT was used to perform the desodiation (oxidation) process and shows that the synthesis takes place via two-phase reaction mechanism at around 0.3-0.4 V vs Na/ Na<sup>+</sup>. The oxidation process can fully convert the Zintl phase precursors into different products depending on the reaction temperature. For Na<sub>4</sub>Ge<sub>4</sub>, the majority of products were type II Ge clathrate, hexagonal  $Na_{1-x}Ge_{3+z}$ , and  $\alpha$ -Ge with a clear low to high temperature (300, 350, and 400 °C, respectively) dependence on the product formation. For the oxidation of Na<sub>4</sub>Ge<sub>3</sub>Si, type II (Ge,Si)<sub>136</sub> clathrate and  $\alpha$ -(Ge,Si) were obtained as single-phase products at 350 and 400 °C, respectively. Rietveld refinement fit the alloyed clathrate phase to a composition of  $Na_{3.4(1)}Si_{34}Ge_{104}$  with a lattice parameter of 15.1129(1) Å. The Na positions were found to adopt off-centered positions in the hexakaidecahedra based on a difference Fourier transform, which was supported by DFT

calculations showing that these positions have lower energy compared to the positions centered within the cages. Finally, NEB calculations showed that Na migration through the clathrate dodecahedra is kinetically difficult with a barrier of 4.0 eV, while Na movement through the hexagonal face between the  $Ge_{28}$  cages is more facile with a migration barrier of 1.3 eV. These results demonstrate that electrochemical oxidation in a cell utilizing a solid electrolyte is effective for the synthesis of Ge clathrate materials from Zintl phase precursors, with the  $Na_4Ge_3Si$  alloyed precursor found to achieve the type II clathrate product with better phase purity.

#### ASSOCIATED CONTENT

#### **Supporting Information**

The Supporting Information is available free of charge at https://pubs.acs.org/doi/10.1021/acs.inorgchem.2c01748.

Detailed experimental procedures for the preparation of Zintl phase precursors, electrochemical reactor assembly, electrochemical measurements, materials characterization, and density functional theory calculations; Rietveld refinement and summary of the crystallographic data and atomic parameters of products; photographs of the stainless-steel and boron nitride reactor housing; and EDS spectra of products (PDF)

#### AUTHOR INFORMATION

#### **Corresponding Author**

Candace K. Chan — Materials Science and Engineering, School for Engineering of Matter, Transport and Energy, Arizona State University, Tempe, Arizona 85827, United States;
ocid.org/0000-0003-4329-4865; Phone: (480) 727-8614; Email: candace.chan@asu.edu

#### **Authors**

Andrew Dopilka — Materials Science and Engineering, School for Engineering of Matter, Transport and Energy, Arizona State University, Tempe, Arizona 85827, United States;
ocid.org/0000-0003-3474-2187

Alexander Ovchinnikov — Department of Chemistry and Biochemistry, University of Delaware, Newark, Delaware 19716, United States; Department of Materials and Environmental Chemistry, Stockholm University, Stockholm 10691, Sweden; orcid.org/0000-0002-0537-4234

Amanda Childs – Department of Chemistry and Biochemistry, University of Delaware, Newark, Delaware 19716, United States

Svilen Bobev — Department of Chemistry and Biochemistry, University of Delaware, Newark, Delaware 19716, United States; orcid.org/0000-0002-0780-4787

Xihong Peng — College of Integrative Sciences and Arts, Arizona State University Polytechnic Campus, Mesa, Arizona 85212, United States

Complete contact information is available at: https://pubs.acs.org/10.1021/acs.inorgchem.2c01748

#### **Author Contributions**

The manuscript was written through contributions of all authors. A.D. designed the electrochemical reactor and performed the electrochemical measurements, materials characterization, and DFT calculations. A.C. and A.D. prepared the Zintl phase compounds. A.O. and S.B. assisted with structure analysis. X.P. assisted with the computational

analysis, and C.K.C. assisted with the electrochemical analysis. All authors have given approval to the final version of the manuscript.

#### Notes

The authors declare no competing financial interest.

#### ACKNOWLEDGMENTS

This work was supported by funding from NSF from the awards DMR-1710017, DMR-1709813, DMR-2004514, and DMR-2004579. A.D. acknowledges support from ASU Fulton Schools of Engineering Dean's Fellowships. The authors acknowledge the use of facilities within the Eyring Materials Center (supported in part by NNCI-ECCS-1542160), the Research Computing Core, as well as the Instrument Design and Fabrication Core Facility at Arizona State University.

#### REFERENCES

- (1) Nolas, G. S.; Beekman, M.; Gryko, J.; Lamberton, G. A.; Tritt, T. M.; McMillan, P. F. Thermal Conductivity of Elemental Crystalline Silicon Clathrate Si<sub>136</sub>. *Appl. Phys. Lett.* **2003**, *82*, 910–912.
- (2) Gryko, J.; McMillan, P. F.; McMillan, P. F.; Marzke, R. F.; Ramachandran, G. K.; Patton, D.; Deb, S. K.; Sankey, O. F. Low-Density Framework Form of Crystalline Silicon with a Wide Optical Band Gap. *Phys. Rev. B* **2000**, *62*, R7707–R7710.
- (3) Martinez, A. D.; Krishna, L.; Baranowski, L. L.; Lusk, M. T.; Toberer, E. S.; Tamboli, A. C. Synthesis of Group IV Clathrates for Photovoltaics. *IEEE J. Photovoltaics* **2013**, *3*, 1305–1310.
- (4) Kume, T.; Ohashi, F.; Nonomura, S. Group IV Clathrates for Photovoltaic Applications. *Jpn. J. Appl. Phys.* **2017**, *56*, No. 05DA05.
- (5) Fix, T.; Vollondat, R.; Ameur, A.; Roques, S.; Rehspringer, J. L.; Chevalier, C.; Muller, D.; Slaoui, A. Silicon Clathrate Films for Photovoltaic Applications. *J. Phys. Chem. C* **2020**, *124*, 14972–14977.
- (6) Moriguchi, K.; Munetoh, S.; Shintani, A. First-Principles Study of Si<sub>34-x</sub>Ge<sub>x</sub> Clathrates: Direct Wide-Gap Semiconductors in Si-Ge Alloys. *Phys. Rev. B* **2000**, *62*, 7138–7143.
- (7) Langer, T.; Dupke, S.; Trill, H.; Passerini, S.; Eckert, H.; Pöttgen, R.; Winter, M. Electrochemical Lithiation of Silicon Clathrate-II. *J. Electrochem. Soc.* **2012**, *159*, A1318–A1322.
- (8) Böhme, B.; Minella, C. B.; Thoss, F.; Lindemann, I.; Rosenburg, M.; Pistidda, C.; Møller, K. T.; Jensen, T. R.; Giebeler, L.; Baitinger, M.; et al. B1-Mobilstor: Materials for Sustainable Energy Storage Techniques—Lithium Containing Compounds for Hydrogen and Electrochemical Energy Storage. *Adv. Eng. Mater.* **2014**, *16*, 1189–1195.
- (9) Dopilka, A.; Weller, J. M.; Ovchinnikov, A.; Childs, A.; Bobev, S.; Peng, X.; Chan, C. K. Structural Origin of Reversible Li Insertion in Guest-Free, Type-II Silicon Clathrates. *Adv. Energy Sustainable Res.* **2021**, *2*, No. 2000114.
- (10) Kasper, J. S.; Hagenmuller, P.; Pouchard, M.; Cros, C. Clathrate Structure of Silicon  $Na_8Si_{46}$  and  $Na_xSi_{136}$  (x <11). Science 1965, 150, 1713–1714.
- (11) Ramachandran, G. K.; Dong, J.; Diefenbacher, J.; Gryko, J.; Marzke, R. F.; Sankey, O. F.; McMillan, P. F. Synthesis and X-Ray Characterization of Silicon Clathrates. *J. Solid State Chem.* **1999**, *145*, 716–730.
- (12) Cros, C.; Pouchard, M.; Hagenmuller, P. Sur Une Nouvelle Famille de Clathrates Mineraux Isotypes Des Hydrates de Gaz et de Liquides. Interpretation Des Resultats Obtenus. *J. Solid State Chem.* 1970, 2, 570–581.
- (13) Baranowski, L. L.; Krishna, L.; Martinez, A. D.; Raharjo, T.; Stevanović, V.; Tamboli, A. C.; Toberer, E. S. Synthesis and Optical Band Gaps of Alloyed Si–Ge Type II Clathrates. *J. Mater. Chem. C* **2014**, *2*, 3231–3237.
- (14) Kume, T.; Ban, T.; Ohashi, F.; Jha, H. S.; Sugiyama, T.; Ogura, T.; Sasaki, S.; Nonomura, S. A Thin Film of a Type II Ge Clathrate Epitaxially Grown on a Ge Substrate. *CrystEngComm* **2016**, *18*, 5630–5638.

- (15) Kumar, R.; Hazama, Y.; Ohashi, F.; Jha, H. S.; Kume, T. A Fabrication Method for Type-II Ge Clathrate Film by Annealing of Ge Film Covered with Na Layer. *Thin Solid Films* **2021**, 734, No. 138859.
- (16) Kumar, R.; Maeda, T.; Hazama, Y.; Ohashi, F.; Jha, H. S.; Kume, T. Growth of Ge Clathrate on Sapphire and Optical Properties. *Jpn. J. Appl. Phys.* **2020**, *59*, No. SFFC05.
- (17) Guloy, A. M.; Ramlau, R.; Tang, Z.; Schnelle, W.; Baitinger, M.; Grin, Y. A Guest-Free Germanium Clathrate. *Nature* **2006**, 443, 320–323
- (18) Guloy, A. M.; Tang, Z.; Ramlau, R.; Böhme, B.; Baitinger, M.; Grin, Y. Synthesis of the Clathrate-II  $K_{8.6(4)}Ge_{136}$  by Oxidation of  $K_4Ge_9$  in an Ionic Liquid. *Eur. J. Inorg. Chem.* **2009**, 2009, 2455–2458
- (19) Böhme, B.; Hoffmann, S.; Baitinger, M.; Grin, Y. Application of N-Dodecyltrimethylammonium Chloride for the Oxidation of Intermetallic Phases. *Z. Naturforsch.*, B: J. Chem. Sci. **2011**, 66, 230–238.
- (20) Feng, X. J.; Lerch, S.; Biller, H.; Micksch, M.; Schmidt, M.; Baitinger, M.; Strassner, T.; Grin, Y.; Böhme, B. Reactivity and Controlled Redox Reactions of Salt-like Intermetallic Compounds in Imidazolium-Based Ionic Liquids. *ChemistryOpen* **2021**, *10*, 205–215.
- (21) Carrillo-Cabrera, W.; Cardoso Gil, R.; Somer, M.; Persil, Ö.; von Schnering, H. G.  $Na_{12}Ge1_7$ : A Compound with the Zintl Anions  $[Ge_4]^{4-}$  and  $[Ge_9]^{4-}$ —Synthesis, Crystal Structure, and Raman Spectrum. *Z. Anorg. Allg. Chem.* **2003**, *629*, 601–608.
- (22) Böhme, B. An Electrochemical Approach toward the Metastable Type II Clathrate Germanium Allotrope. *Inorg. Chem.* **2020**, *59*, 11920–11924.
- (23) Dopilka, A.; Childs, A.; Bobev, S.; Chan, C. K. Solid-State Electrochemical Synthesis of Silicon Clathrates Using a Sodium-Sulfur Battery Inspired Approach. *J. Electrochem. Soc.* **2021**, *168*, No. 020516.
- (24) Reed, D.; Coffey, G.; Mast, E.; Canfield, N.; Mansurov, J.; Lu, X.; Sprenkle, V. Wetting of Sodium on  $\beta''$ -Al<sub>2</sub>O<sub>3</sub>/YSZ Composites for Low Temperature Planar Sodium-Metal Halide Batteries. *J. Power Sources* **2013**, 227, 94–100.
- (25) Weppner, W.; Huggins, R. A. Determination of the Kinetic Parameters of Mixed-Conducting Electrodes and Application to the System Li<sub>3</sub>Sb. *J. Electrochem. Soc.* 1977, 124, No. 1569.
- (26) Peng, X.; Wei, Q.; Li, Y.; Chan, C. K. First-Principles Study of Lithiation of Type I Ba-Doped Silicon Clathrates. *J. Phys. Chem. C* **2015**, *119*, 28247–28257.
- (27) Dopilka, A.; Zhao, R.; Weller, J. M.; Bobev, S.; Peng, X.; Chan, C. K. Experimental and Computational Study of the Lithiation of Ba<sub>8</sub>Al<sub>y</sub>Ge<sub>46-y</sub> Based Type I Germanium Clathrates. *ACS Appl. Mater. Interfaces* **2018**, *10*, 37981–37993.
- (28) Dopilka, A.; Peng, X.; Chan, C. K. Ab Initio Investigation of Li and Na Migration in Guest-Free, Type I Clathrates. *J. Phys. Chem. C* **2019**, *123*, 22812–22822.
- (29) Henkelman, G.; Uberuaga, B. P.; Jónsson, H. Climbing Image Nudged Elastic Band Method for Finding Saddle Points and Minimum Energy Paths. *J. Chem. Phys.* **2000**, *113*, 9901–9904.
- (30) Huggins, R. A. Advanced Batteries: Materials Science Aspects; Springer: Boston, 2008.
- (31) Chevrier, V. L.; Ceder, G. Challenges for Na-Ion Negative Electrodes. J. Electrochem. Soc. 2011, 158, 1011–1014.
- (32) Feng, X.; Bobnar, M.; Lerch, S.; Biller, H.; Schmidt, M.; Baitinger, M.; Strassner, T.; Grin, Y.; Böhme, B. Type-II Clathrate  $Na_{24-\delta}Ge_{136}$  from a Redox-Preparation Route. *Chem. Eur. J.* **2021**, 136, 12776–12787.
- (33) Beekman, M.; Kaduk, J. A.; Huang, Q.; Wong-Ng, W.; Yang, Z.; Wang, D.; Nolas, G. S. Synthesis and Crystal Structure of  $Na_{1-x}Ge_{3+2}$ : A Novel Zeolite-like Framework Phase in the Na-Ge System. *Chem. Commun.* **2007**, *8*, 837–839.
- (34) Peckham, G. D.; McNaught, I. J. The Variation of Electrochemical Cell Potentials with Temperature. *J. Chem. Educ.* **2011**, *88*, 782–783.
- (35) Beekman, M.; Stefanoski, S.; Wong-Ng, W.; Kaduk, J. A.; Huang, Q.; Reeg, C.; Bowers, C. R.; Nolas, G. S. Structure and

Thermal Conductivity of  $Na_{1-x}Ge_{3+z}$ . J. Solid State Chem. **2010**, 183, 1272–1277.

- (36) Jakobsen, H. J.; Bildsøe, H.; Beekman, M.; Stefanoski, S.; Nolas, G. S.; Bowers, C. R. Low-Temperature <sup>23</sup>Na MAS NMR Reveals Dynamic Effects and Compositions for the Large and Small Channels in the Zeolite-like Ge-Framework of Na<sub>1-x</sub>Ge<sub>3+z</sub> Materials. *J. Phys. Chem. C* **2014**, *118*, 28890–28897.
- (37) Beekman, M.; Baitinger, M.; Borrmann, H.; Schnelle, W.; Meier, K.; Nolas, G. S.; Grin, Y. Preparation and Crystal Growth of Na<sub>24</sub>Si<sub>136</sub>. *J. Am. Chem. Soc.* **2009**, *131*, 9642–9643.
- (38) Beekman, M.; Nenghabi, E. N.; Biswas, K.; Myles, C. W.; Baitinger, M.; Grin, Y.; Nolas, G. S. Framework Contraction in Na-Stuffed Si (*cF*136). *Inorg. Chem.* **2010**, *49*, 5338–5340.
- (39) Slingsby, J. G.; Rorrer, N. A.; Krishna, L.; Toberer, E. S.; Koh, C. A.; Maupin, C. M. Dynamic Free Energy Surfaces for Sodium Diffusion in Type II Silicon Clathrates. *Phys. Chem. Chem. Phys.* **2016**, 18, 5121–5128.
- (40) Yang, J.; Tse, J. S. Silicon Clathrates as Anode Materials for Lithium Ion Batteries? *J. Mater. Chem. A* **2013**, *1*, 7782–7789.
- (41) Morito, H.; Momma, K.; Yamane, H. Crystal Structure Analysis of Na<sub>4</sub>Si<sub>4-x</sub>Ge<sub>x</sub> by Single Crystal X-Ray Diffraction. *J. Alloys Compd.* **2015**, *623*, 473–479.

### **□** Recommended by ACS

### **Blade-Type Reaction Front in Micrometer-Sized Germanium Particles during Lithiation**

Xinwei Zhou, Likun Zhu, et al.

SEPTEMBER 28, 2020

ACS APPLIED MATERIALS & INTERFACES

READ 🗹

#### (De)Lithiation and Strain Mechanism in Crystalline Ge Nanoparticles

Diana Zapata Dominguez, Stéphanie Pouget, et al.

MAY 25, 2022

ACS NANO

READ 🗹

#### 2D Silicon-Germanium-Layered Materials as Anodes for Li-Ion Batteries

Xi Chen, Vincent Seznec, et al.

NOVEMBER 10, 2021

ACS APPLIED ENERGY MATERIALS

READ 🗹

## Understanding the Amorphous Lithiation Pathway of the Type I Ba<sub>8</sub>Ge<sub>43</sub> Clathrate with Synchrotron X-ray Characterization

Andrew Dopilka, Candace K. Chan, et al.

OCTOBER 20, 2020

CHEMISTRY OF MATERIALS

READ 🗹

Get More Suggestions >